Journal of
Manufacturing and Materials Processing

MDPI

Article

An Experimental–Numerical Framework for Springback Prediction and Angle Compensation in Air Bending with Additively Manufactured Polymer Tools

Vesna Mandic *, Marko Delic, Dragan Adamovic, Dusan Arsic, Nada Ratkovic, Djordje Ivkovic and Andjelka Ilic

Faculty of Engineering, University of Kragujevac, 34000 Kragujevac, Serbia; marko.delic@kg.ac.rs (M.D.); adam@kg.ac.rs (D.A.); dusan.arsic@fink.rs (D.A.); nratkovic@kg.ac.rs (N.R.); djordje.ivkovic@fink.rs (D.I.); andjelka.ilic@fink.rs (A.I.)

* Correspondence: mandic@kg.ac.rs; Tel.: +381-34-501201

Abstract

Additive manufacturing of polymer tools represents a promising alternative to conventional steel tooling for low-force and low-volume sheet metal air bending. However, accurate prediction of sheet springback and the resulting deviation of the bending angle after elastic unloading remains a major challenge. This study presents an integrated experimental–numerical framework for the analysis of air bending with additively manufactured polymer tools, with emphasis on material characterization, springback prediction, and tool angle compensation. The methodology combines uniaxial tensile testing, controlled air-bending experiments, finite element modelling with rigid and deformable tools, and optical 3D scanning for angle measurement. Low-carbon steel DC04 sheets were modeled using an elastoplastic constitutive law, while additively manufactured ABS tools were described by experimentally calibrated material models. Numerical simulations were performed over a range of forming forces to evaluate springback behavior and elastic tool deformation. The results show very good agreement between experiments and simulations. Deviations in bending angle were below 1.5% for metallic tools and below 0.5% for springback compensation, with the smallest discrepancy obtained using a two-dimensional model with deformable tools. Experimental validation with ABS tools confirmed bending accuracy within $\pm 1^{\circ}$. The proposed framework provides a reliable basis for springback prediction and rational design of additively manufactured polymer tools for air-bending applications.

Keywords: additive manufacturing; polymer tools; air bending; springback prediction; finite element modelling; ABS; sheet metal forming

Academic Editor: Guido Di Bella

Received: 22 December 2025
Revised: 8 January 2026
Accepted: 9 January 2026
Published: 11 January 2026

1. Introduction

Additive manufacturing (AM) of polymer tools has opened new possibilities for flexible and cost-effective sheet metal forming, especially in small and medium enterprises (SMEs) and in low-volume or prototype production. Conventional toolmaking based on hardened steel or cast-iron dies is still the standard for high-volume stamping and deep drawing, but it involves long lead times, expensive machining, and limited adaptability once the tooling is finished. In contrast, direct additive tooling, typically based on fused deposition modelling/filament fabrication (FDM/FFF, MEX—Material Extrusion in line with ISO/ASTM 52900 global standard for additive manufacturing [1]), enables direct fabrication of forming tools from CAD data, with minimal material waste and very low

material cost, making it attractive for rapid tooling, design iterations, and short production runs [2–4].

The feasibility of using polymer tools in metal forming has been demonstrated in several processes. Durgun investigated polymer upper and lower dies for stamping prototype parts from DC04 and S355MC steel, and showed that, for DC04, up to about 100 parts can be produced within the dimensional tolerances, with significant reductions in tool cost and lead time compared to conventional tooling [3]. Nakamura et al. evaluated plastic tools produced by MEX for both V-bending and deep drawing of steel and aluminium sheets, and highlighted that dimensional accuracy is limited by the low stiffness of the plastic tools, but can be improved by reinforcing the tools with steel bars and by modifying the tool geometry to compensate for elastic deformation and springback [2]. They also showed that plastic dies can be particularly advantageous in deep drawing of softer sheet materials, because they reduce scratching and allow forming without lubrication. Complementary to these feasibility studies, Kaleem et al. proposed a design criterion for 3D printed polymer tools in metal forming, based on a von Mises failure approach. Their combined FE–experimental analysis provides a practical way for SMEs to assess whether a given polymer tool geometry and material will safely carry the forming load, even when only engineering stress–strain data from standard tensile tests are available [5].

Beyond bending and deep drawing, polymer-based rapid tooling has been explored for hydroforming, groove pressing, and more complex parts. Prithvirajan et al. used printed ABS dies as direct rapid tools for metal bellow hydroforming and showed, via combined FEA and experiments, that such dies can successfully form stainless steel bellows in low-volume production. They also demonstrated how low-stress regions in the die can be topologically modified (e.g., by introducing pores or lattice structures) to reduce material consumption, provided that the die strength remains above the critical level [6]. Tondini et al. evaluated additively manufactured polymer tools in V-bending and groove pressing of 1 mm aluminium sheets. Their results showed that additively manufactured polymer tools reach a steady-state surface condition after a few strokes, and that the combination of springback and elastic deflection of the tools significantly influences the final bend angle; however, the scatter of the resulting geometry is low enough to allow systematic tool corrections toward nominal values [7]. In a related study, the same group proposed a flexible production concept in which 3D printed PLA tools are used in a multi-feature forming operation, and compared the time and cost of printed tools to conventionally machined tools. They concluded that, for small series and flexible manufacturing, printed tools can be produced overnight at a fraction of the cost, and that PLA tools also offer environmental benefits such as recyclability and reduced need for lubricants [8].

Additive tooling is not limited to metal forming. Popović et al. presented an integrated use of reverse engineering and additive manufacturing for rapid tooling in two-component polymer casting. Based on optical scanning of an existing plastic part, they built and iteratively refined a master CAD model and printed casting tools. The successful replication of the original gas-handle geometry confirmed that AM-based rapid tooling can shorten development time and reduce cost in small-batch polymer processing when technical documentation is missing [3]. These studies collectively show that additive tooling has matured into a versatile concept applicable to deep drawing, hydroforming, air bending, groove pressing, and casting, and that it is particularly suitable when flexibility, low investment, and short lead time are more important than tool life in the millions of cycles [2–4,6–8].

A number of works have focused specifically on bending processes with polymer tools and on the associated stress–strain states. Rehman analysed U- and V-shaped tools made of PLA, combining static structural analysis in ANSYS (R15.0) with experimental

V-bending tests. The study confirmed that plastic tools can be used for sheet metal bending with acceptable dimensional accuracy, reduced fixed tooling cost, and reduced material waste, especially in small batches [9]. Giorleo and Deniz investigated V-bending of 2 mm stainless steel sheets using MEX tools made of nylon reinforced with short carbon fibres. By comparing horizontal and vertical build orientations, they showed that polymer punches and dies undergo measurable permanent deformation away from the working zone, yet are capable of maintaining sheet geometry within 0.5% deviation over multiple cycles [10]. Zaragoza et al. examined V-die air bending using PC and PLA dies produced by MEX AM technology. They performed compression tests on printed samples with different printing strategies, used FE simulations to identify critical tool regions, and carried out repeated bending tests. Their results highlighted the strong influence of printing pattern on tool stiffness, durability and angle repeatability. Among the tested configurations, a 45–90–45° printing pattern for PLA dies provided a particularly stable bending response over many cycles [11].

At the same time, there has been considerable progress in the mechanical characterization of AM polymers specifically for tool design. Frohn-Sörensen et al. systematically evaluated compressive and flexural properties of different FFF polymers and layer heights, and used the resulting data as input for a cup-drawing case study. Their work illustrates how accurate mechanical characterization of solid-infill specimens can support a more reliable design of DPAT (Direct Polymer Additive Tooling) tools under high forming loads [12]. However, the mechanical response of printed polymers is not only material-dependent but also highly sensitive to process parameters and internal architecture. Hmeidat et al. quantified the effect of infill patterns on the stiffness, strength, and failure modes of topologically optimized ABS beams in three-point bending, showing up to 22% variation in stiffness and a 426% variation in failure load between different patterns. Their elastic FEA with orthotropic plies captured stiffness trends well, but simple maximum-stress criteria were insufficient to predict strength, underscoring the complexity of failure in printed structures [13]. El-Deeb et al. studied the influence of nozzle diameter and printing speed on the tensile behaviour of ABS and PLA and found that optimal combinations of large nozzle diameter and moderate speed can significantly improve tensile strength, with PLA generally outperforming ABS but also being more sensitive to process windows [14].

The nonlinear and anisotropic behaviour of ABS in MEX AM has been investigated in more detail by Bhuiyan and Khanafer, who combined uniaxial tensile tests at different infill densities with hyperelastic modelling. They showed that Young's modulus increases exponentially with infill density and that strain at break exhibits a non-monotonic trend, while hyperelastic models such as Mooney–Rivlin and Yeoh can accurately reproduce the observed stress–strain curves. This provides a basis for more realistic constitutive models of printed ABS in FE simulations [15]. Complementing these generic studies, our research group has carried out extensive experimental work on ABS materials for forming tools. In tensile tests, Delic et al. showed that raster angle, layer thickness, printing velocity, infill pattern, and infill density all significantly affect tensile strength and strain at break, with the most favourable combinations involving a $\pm 45^{\circ}$ raster angle, thin layers, and high infill, but these settings substantially increase printing time [16]. Overall, these results confirm that mechanical properties of candidate polymer tool materials are highly process-dependent and must be carefully characterized and selected for each application.

On the modelling side, there is a well-established body of work on numerical simulation of metal forming processes, including springback prediction, but its systematic integration with polymer tooling is still limited. Mandic provided a comprehensive framework for physical and numerical modelling of metal forming, including constitutive modelling, contact behaviour, and validation strategies, which is widely applicable to both conven-

tional tools and additively manufactured [17]. Aksenov and Kononov demonstrated that numerical simulation of sheet metal forming with plastic tools in Simufact.forming can accurately capture forming forces, stress distribution in the tool, and the springback of aluminium parts, thereby confirming the feasibility of using 3D printed plastic tools for thin-sheet forming when tool stresses remain below the elastic limit [18]. Kella and Mallick analysed springback in aluminium/polypropylene/aluminium sandwich laminates, combining LS-DYNA simulations with experiments and systematically studying the influence of sheet thickness, die and punch radius, and blank holder force. Their work showed how process parameters and laminate design can be tuned to control springback, but focused on metallic/composite sheets with conventional steel tools [19].

More recently, topology optimization and advanced FE modelling have been applied to polymer tools themselves. Giorleo and Deniz proposed a topology-optimization-based design of polymer bending tools produced by MEX. They used standard polymer tools to identify load conditions, performed topology optimization to reduce tool mass by about 50%, and validated the optimized geometry experimentally. The optimized tools exhibited increased elastic deformation and slightly larger springback ($\approx 2^\circ$ difference in bending angle), but remained structurally safe and functionally adequate for low-volume production [20]. Bhatia and Patel, in turn, combined FE simulation and experiments for V-bending with ABS tools, evaluating formability and dimensional accuracy for SS304 and AA6061 sheets and indicating that ABS tools can be loaded up to about 139 MPa in compression with acceptable wear over on the order of 100 parts [21]. These studies demonstrate that detailed FE modelling of sheet metal forming with polymer tools is feasible and that topology optimization can further improve AM efficiency, but they generally stop at demonstrating feasibility or mass reduction, with limited emphasis on predictive control of springback and on systematic comparison between polymer and steel tools for industrially relevant air-bending operations.

Despite this substantial progress, several important research gaps remain. First, many experimental studies on polymer tools primarily demonstrate feasibility for selected low-volume forming applications, often considering a limited range of bending angles, sheet thicknesses, or materials, while springback compensation is frequently treated empirically rather than through predictive numerical models. Second, although the mechanical behaviour of additively manufactured polymers is known to be strongly influenced by printing parameters, infill characteristics, and reinforcement strategies, this knowledge is only partially transferred into forming simulations. In many cases, material models are derived from simple standardized test specimens and do not fully represent the complex combination of compression, bending, and cyclic loading experienced by forming tools during air bending. Third, fully integrated frameworks that combine systematic material characterization of both sheet metal and polymer tools, finite element simulation accounting for elastic deformation of both components, and high-resolution experimental validation of springback remain scarce for air-bending processes.

This study proposes a comprehensive experimental–numerical framework for the analysis of air bending of sheet metal with additively manufactured polymer tools. The focus is placed on accurate characterization of material behaviour, reliable prediction of springback, and numerical determination of tool angle compensation required to achieve the target bending geometry. The proposed methodology integrates uniaxial tensile testing, controlled air-bending experiments, finite element modelling, and optical angle measurement, providing a consistent basis for validation of numerical predictions.

The presented approach systematically combines experiments performed with conventional steel tools and numerical simulations using rigid and deformable tools to establish a validated reference model of the air-bending process. This validated framework is subse-

quently extended to simulations and experiments with additively manufactured ABS tools, enabling assessment of the influence of reduced tool stiffness on the resulting bending angle and verification of the proposed springback compensation strategy.

Building on previous investigations of the tensile and compressive behaviour of MEX-printed ABS under varying raster orientations, infill patterns, densities, and layer thicknesses, the relevant mechanical response of the tool material is characterized for the stress state encountered in air bending. These data are used to calibrate constitutive models for the polymer tools, while established elastoplastic models are adopted for mild steel sheets, following best practices in numerical simulations of sheet metal forming [17].

Finite element analyses of the air-bending process are performed with explicit consideration of the elastic–plastic response of the sheet material and the influence of tool stiffness on the bending process, enabling accurate prediction of sheet springback. The numerical results are validated through controlled bending experiments and high-resolution optical measurements of the bent geometry. Through this integrated approach, the study provides a validated basis for numerical springback prediction and tool angle compensation, and establishes methodological guidelines for the rational design and assessment of additively manufactured polymer tools for low-force air-bending applications.

2. Materials and Methods

2.1. Sheet Material

The sheet material investigated in this study was low-carbon cold-rolled steel DC04, chosen for its good formability and stable mechanical response, which make it suitable for systematic experimental and numerical analysis of bending processes. The sheets were supplied in cold-rolled condition with a nominal thickness of t = 0.8 mm.

In order to ensure accurate numerical simulation of the air-bending process and reliable springback prediction, the mechanical behaviour of the sheet material was characterized experimentally through uniaxial tensile testing. Uniaxial tensile tests were conducted at room temperature in accordance with ISO 6892-1 [22]. Standard flat specimens were prepared by laser cutting, with three different orientations relative to the rolling direction (0°, 45°, and 90°), in order to capture potential anisotropy effects. The specimen geometry and cutting directions are shown in Figure 1.

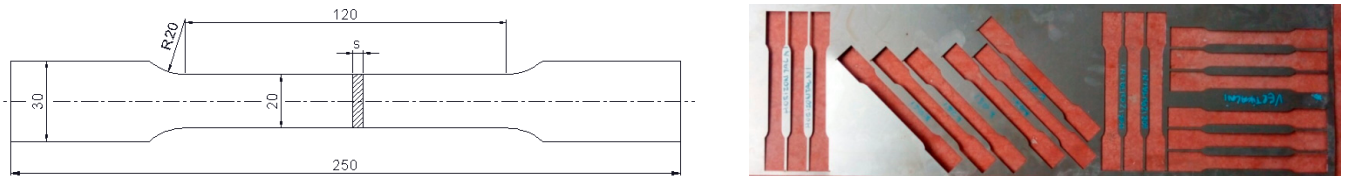

(**a**) (**b**)

Figure 1. Specimen geometry (**a**) and cutting directions (**b**).

The experiments were performed on a Shimadzu universal testing machine (Shimadzu Corporation1-1, Kyoto, Japan) located at the Faculty of Engineering. The testing system was equipped with pneumatic grips and a mechanical extensometer with a gauge length of 50 mm, enabling accurate measurement of axial strain during loading. A photograph of the testing setup and the mounted specimen is shown in Figure 2.

(**a**) (**b**)

Figure 2. Testing setup: (**a**) Shimadzu universal testing machine; (**b**) mounted specimen.

The crosshead speed was determined according to the recommendations of ISO 6892-1 [22], based on the selected gauge length and target strain rate in the elastic–plastic transition region. Following the standard procedure and the prescribed strain rate range, a nominal crosshead speed of 2 mm/min was adopted for all experiments. This ensured stable deformation conditions and reliable identification of yield and hardening behaviour.

Representative engineering stress–strain curve obtained from the tensile tests is presented in Figure 3. The corresponding mechanical properties, including yield stress R_p, ultimate tensile strength R_m, and total elongation at fracture A_{120} (with L_0 = 120 mm) are summarized in Table 1. The results show a moderate dependence of yield stress on specimen orientation, with the highest yield stress observed for specimens cut along the rolling direction. In contrast, the ultimate tensile strength remained nearly identical for the 0° and 45° orientations and slightly lower for specimens cut at 90°, indicating limited anisotropy in tensile strength.

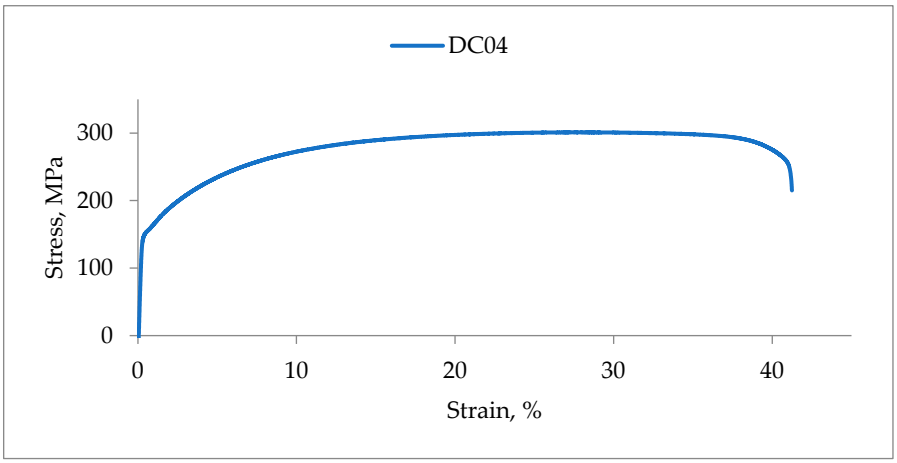

Figure 3. Stress–strain curve for DC04 (rolling direction).

Table 1. DC04 mechanical properties.

Angle	Rp, MPa	Rm, MPa	A_{120}, %
0°	151	301	40.87
45°	158	311	39.06
90°	153	290	39.90

For numerical modelling of the air-bending process, the flow stress curve of DC04 was determined experimentally from the tensile test data. The analysis focused on the region of homogeneous plastic deformation, between the onset of yielding and the maximum tensile force. The experimentally obtained true stress–true strain data were approximated using a least-squares fitting procedure, implemented in Statistica (v14.0) and Microsoft Excel (v11). The resulting analytical representation of the flow curve is shown in Figure 4 and can be expressed in power-law form as

$$\sigma = 542.66 \cdot \varphi^{0.2259} \quad (1)$$

The quality of the approximation was confirmed by a high correlation coefficient (R^2 = 0.996), indicating excellent agreement between experimental data and the fitted model.

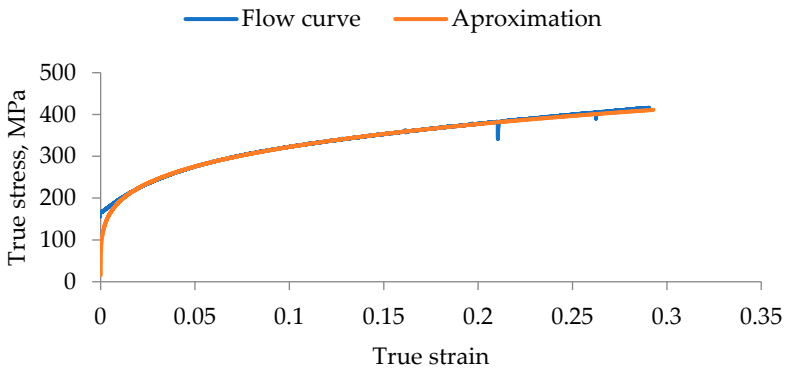

Figure 4. Flow curve for DC04.

The identified flow curve parameters were used directly as input for the finite element simulations of the air-bending process. For springback prediction, the sheet material was modelled as elastoplastic with isotropic hardening, which is a commonly adopted and well-established approach in numerical simulations of sheet metal forming processes [17]. This material characterization provided a reliable basis for coupling experimental bending tests with finite element analysis and for accurately predicting elastic springback of the sheet and the resulting final bent geometry.

2.2. Tool Material and Additive Manufacturing

The bending tools used in this study were manufactured from acrylonitrile–butadiene–styrene (ABS) using material extrusion (MEX) and 3D printer MakerBot Replicator 2X (MakerBot Industries, LLC., New York, NY, USA). ABS was selected due to its widespread availability, low material cost, good printability, and a favourable balance between stiffness and ductility, which makes it suitable for low-force and low- to medium-volume forming applications.

The mechanical behaviour of MEX-printed ABS is strongly dependent on printing parameters such as raster angle, layer thickness, infill pattern, infill density, and build orientation. A comprehensive experimental investigation of these effects, including tensile and compressive testing and fracture analysis, was previously conducted by the authors and reported in detail in [16].

In that study, it was demonstrated that raster orientation, layer thickness, and infill architecture have a pronounced influence on tensile strength, strain at break, and fracture mode of ABS specimens. In particular, raster angles of ±45°, reduced layer thickness, and high infill densities were shown to provide improved mechanical performance, although at the expense of increased printing time. Complementary compression tests further indicated that vertical build orientation, small layer thickness, and rectangular infill patterns yield higher compressive strength, which is directly relevant for the predominantly compressive loading conditions encountered in air-bending tools.

In addition to the previously published experimental investigation [16], a statistical analysis was performed in order to quantitatively assess the relative influence of selected MEX printing parameters that are particularly relevant for bending tools, namely raster orientation and layer thickness. While the initial analysis of tensile results was based on averaging procedures, a more rigorous evaluation of parameter significance requires the application of dedicated statistical methods.

For this purpose, the Taguchi method was employed. For each experimental run, the signal-to-noise (S/N) ratio was calculated and used as the objective function for optimization. The S/N ratio represents a logarithmic transformation of the output response and enables robust comparison of parameter effects by reducing the influence of random variability. Since the objective was to maximize tensile strength, the "larger-is-better" criterion was adopted.

A Taguchi L9 orthogonal array was selected, considering two control factors, raster orientation (U) and layer thickness (s), each at three levels. The experimental plan and the corresponding tensile strength values and S/N ratios are summarized in Table 2. Statistical analysis was carried out using Minitab (v22.4.0) [23].

Table 2. Experimental plan, tensile strength values and S/N ratios for MEX-printed ABS.

Run	U	s	Rm, MPa	S/N
1	U1 (0°/90°)	S1(0.1 mm)	37.19	31.4085
2	U1 (0°/90°)	S2(0.2 mm)	35.64	31.0388
3	U1 (0°/90°)	S3(0.3 mm)	35.15	30.9185
4	U3 (30°/60°)	S1(0.1 mm)	39.35	31.8989
5	U3 (30°/60°)	S2(0.2 mm)	36.78	31.3122
6	U3 (30°/60°)	S3(0.3 mm)	38.55	31.7205
7	U4 (45°/−45°)	S1(0.1 mm)	40.38	32.1233
8	U4 (45°/−45°)	S2(0.2 mm)	38.98	31.8168
9	U4 (45°/−45°)	S3(0.3 mm)	38.92	31.8035

Mean S/N values were calculated for each factor level, and the Delta value was determined as the difference between the maximum and minimum mean S/N ratios for a given factor. The factor with the highest Delta value was ranked as the most influential. The results clearly indicate that raster orientation has a stronger influence on tensile strength than layer thickness. Specifically, the raster orientation factor exhibited a Delta value of 0.79, compared to 0.42 for layer thickness, corresponding to ranks 1 and 2, respectively.

To further quantify the relative importance of the parameters, an analysis of variance (ANOVA) was performed on the S/N ratios. The percentage contribution of each factor was calculated based on the ratio of its sum of squares to the total sum of squares. The analysis showed that raster orientation accounts for approximately 71.6% of the total variation in tensile strength, whereas layer thickness contributes 21.7%. These results confirm that raster orientation is the dominant parameter governing the tensile behaviour of MEX-printed ABS, which is particularly important for bending tools subjected to combined compressive and bending loads.

Based on these findings, ABS was adopted in the present work as a representative polymer tool material, and printing parameters were selected to ensure sufficient stiffness and load-bearing capacity while maintaining reasonable manufacturing time. The previously established material characterization [16] therefore serves as the mechanical basis for the numerical modelling and experimental evaluation of additively manufactured bending tools presented in this study.

For finite element modelling of air bending with polymer tools, a constitutive description of the ABS material was required. The analysis focused on specimens printed with 100% infill, a ±45° raster orientation, and a layer thickness of 0.2 mm, which represents a commonly used and mechanically favourable printing configuration for functional tools. Printing speed was kept constant, as previous analysis showed that its influence on mechanical properties is negligible compared to raster orientation and layer thickness [15]. All printed specimens were subjected to a tensile test in accordance ASTM D638 standard [22], on a universal testing machine ZWICK/Roell Z100 (ZwickRoell Am Gansacker 1, Ulm, Germany) at room temperature. The tensile tests were performed at a displacement-controlled loading rate of 1.3 mm/min. A ceramic extensometer in the range of 11–50 mm is used to measure specimen elongation, which facilitates direct measurement of changes in the length of the specimen. During the test, data is collected automatically, as pairs of load force and elongation values, by means of testXpert software (vIII), with a data acquisition speed of 500 Hz. The same software uses the collected data to calculate the strain, strain at break, yield strength and tensile strength. The experimentally obtained tensile stress–strain curves indicate a predominantly a quasi-brittle mechanical response characterized by limited plastic deformation prior to fracture. The following mechanical properties were obtained from tensile testing: yield stress Rp = 38.24 MPa, ultimate tensile strength Rm = 38.98 MPa and fracture strain ε_f= 6.67%.

Based on the results of tensile testing, the flow stress behaviour of ABS was described using a power-law hardening model of the form $\sigma = C\varphi^n$, where σ is the true stress, φ is the true plastic strain, C is the strength coefficient, and n is the strain-hardening exponent. Using least-squares fitting of the true stress–true strain data in the homogeneous deformation region, the material constants were identified as: C = 1314.59 and n = 1.073. The resulting flow stress curve and its analytical approximation are shown in Figure 5. The identified parameters provide an adequate description of the nonlinear mechanical response of MEX-printed ABS and were directly implemented in the finite element simulations of the air-bending process.

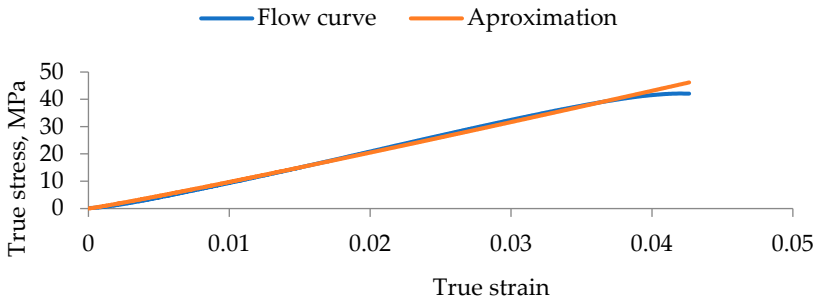

Figure 5. Flow curve for MEX-printed ABS.

This combined experimental and statistical characterization ensures that the constitutive model used for the polymer tools reflects both the dominant influence of printing parameters and the actual stress–strain behaviour relevant to tool loading conditions in air bending.

2.3. Tool Geometry and Air-Bending Configuration

2.3.1. Specimen Geometry

Prior to tool design and experimental planning, the admissible bending radius range and the developed blank length were estimated in order to define the target geometry of the V-bent specimen. The nominal dimensions of the bent part are shown in Figure 6. This geometry was selected to ensure a uniform bending zone and to allow reliable comparison between experimental measurements and numerical predictions under plane-strain conditions. The specimen dimensions are representative of typical laboratory-scale air-bending tests and are sufficiently large to avoid edge effects while remaining compatible with the available tooling and testing machine constraints. The air-bending experiments were performed on rectangular sheet specimens made of DC04 steel, with dimensions 35 × 60 mm and a nominal thickness of 0.8 mm.

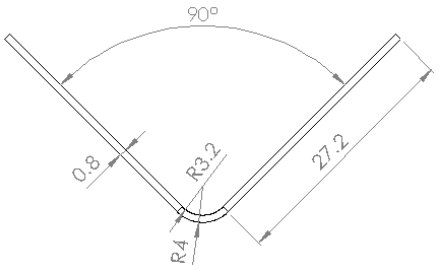

Figure 6. Nominal dimensions of the bent part.

2.3.2. Air-Bending Tool Configuration

A dedicated modular air-bending tool was used in the experiments, mounted on a universal testing machine (Zwick/Roell Z100). The tool was designed to ensure accurate alignment of the punch, die, and sheet specimen, as well as repeatable boundary conditions during bending. The working elements of the bending tool (die and punch) are made of tool steel C60. A representative view of the tool mounted on the testing machine is shown in Figure 7.

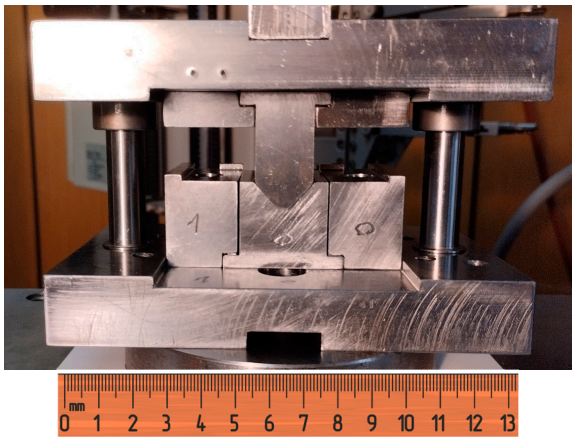

Figure 7. Air-bending tool mounted on the testing machine Zwick Roell Z100.

The modular tool concept enables rapid replacement of conventional steel punch and die elements with additively manufactured ABS inserts, allowing direct experimental comparison of metal and polymer tools under identical loading and boundary conditions. Air-bending experiments with metallic punch and die inserts were conducted to establish a reference springback response of the sheet material under rigid tooling conditions. These experiments served to validate the finite element model of the process and to determine

the required compensation angle for achieving the target bend geometry. Based on this validated numerical framework, additively manufactured ABS tools with compensated geometries were subsequently designed and tested, allowing verification of the predicted bending angle under identical forming conditions.

2.3.3. Loading Scheme and Process Parameters

The air-bending experiments were conducted under force-controlled conditions, with the maximum forming force prescribed as the primary control parameter. Four force levels were selected: 600 N, 1000 N, 1500 N, and 2000 N. This range was chosen to cover low to moderate forming severities, which are particularly relevant for polymer-based bending tools, where excessive forming forces must be avoided to prevent tool damage. The selected loading scheme provides a controlled framework for identifying the relationship between forming force and springback angle, which is essential for validation of the numerical model and for subsequent determination of springback compensation strategies. The maximum force was defined in the TestXpert control software (vIII) of the testing machine. Once the prescribed force level was reached, punch motion was stopped and unloading was initiated, allowing elastic recovery of the sheet. All experiments were carried out at a constant crosshead speed of 5 mm/min, ensuring quasi-static conditions and stable force–displacement response.

2.4. Finite Element Modelling of Air Bending

Finite element simulations of the one-angle air-bending process were performed using the commercial software Simufact.forming (v15) [24], which employs the MSC Marc solver. The numerical modelling was carried out in two stages: first using rigid tools and subsequently using deformable tools, in order to assess the influence of tool elastic deflection on springback behaviour. For simulations involving deformable tools, a finite element mesh was also generated for the punch and die. The tools were discretized using an advancing front quadrilateral mesh with Quad 11 elements. A nominal element size of 2 mm was adopted for the tool bodies. In order to accurately capture local stress and deformation gradients in regions of intensive tool–sheet interaction, the mesh was locally refined in the contact zones by a refinement factor of four. This approach ensured sufficient numerical accuracy in the prediction of elastic tool deformation while maintaining reasonable computational efficiency.

Material anisotropy of the sheet was taken into account by defining the rolling direction and anisotropy coefficients r = 1,54. The Hill anisotropic yield criterion was employed.

The bending process was modelled as a 2D planar problem, which is commonly adopted for air bending due to the constant cross-section along the bending length. The sheet was discretized using quadrilateral finite elements generated with an advancing-front meshing strategy. An element size of 0.15 mm was adopted in the bending zone to accurately capture strain gradients.

Contact between the sheet and the tools was modelled using a Coulomb friction law, with a friction coefficient of 0.1, selected from the Simufact material library (*sheet_medium* condition). All simulations were performed at room temperature (20 °C), consistent with the experimental conditions.

2.5. Springback Evaluation

2.5.1. Numerical Springback Evaluation

Springback in the numerical simulations was evaluated after complete unloading and removal of the tools. The total strain state, consisting of elastic and plastic components, was monitored during the unloading phase. Tool removal and workpiece release were defined using the *Release dies attached to press* and *Release workpiece from stationary dies*

options. Elastic recovery was simulated incrementally over ten unloading steps to improve numerical stability.

The deformed sheet geometry after unloading was exported in STL format and evaluated in CATIA CAD software (v6) to determine the predicted bending angle of the virtual bent part. These numerical predictions were later compared with experimental measurements to verify the accuracy of the material model and boundary conditions.

This numerical procedure enables direct assessment of elastic recovery as a function of forming force and provides a quantitative basis for comparison with experimental measurements.

2.5.2. Experimental Springback Measurement by Optical 3D Scanning

Experimental evaluation of springback was performed using optical 3D scanning based on structured light projection. A DAVID SLS-2 scanner (DAVID Vision Systems GmbH, Koblenz, Germany) was employed, consisting of a projector and camera system that reconstructs object geometry from projected light patterns [25]. Prior to scanning, the scanner was calibrated using a reference calibration panel, and the surfaces of the bent sheet specimens were lightly matted to improve optical contrast. The specimens were scanned from multiple orientations, and the resulting point clouds were processed in dedicated inspection software.

The bending angle was determined by extracting a cross-section from the point cloud and fitting reference lines to the planar regions of the sheet legs. This non-contact measurement approach provides high repeatability and sufficient accuracy for springback assessment and for validation of numerical predictions. The performance characteristics of the DAVID structured-light scanning system have been reported in the literature and are suitable for sheet-metal metrology applications.

3. Results

3.1. Experimental–Numerical Air-Bending Results with Metallic Tools

3.1.1. Experimental Air-Bending with Metallic Tools

In order to identify the springback behaviour of the sheet material independently of elastic deformation of the tools, air-bending experiments were first performed using conventional metallic punch and die inserts. The punch had a nose radius of 3.2 mm and an opening angle of 89°, while the die radius was 4 mm with a die angle of 90°. The experimental setup, including the mounted tool and the sheet specimen before and after bending, is shown in Figure 8.

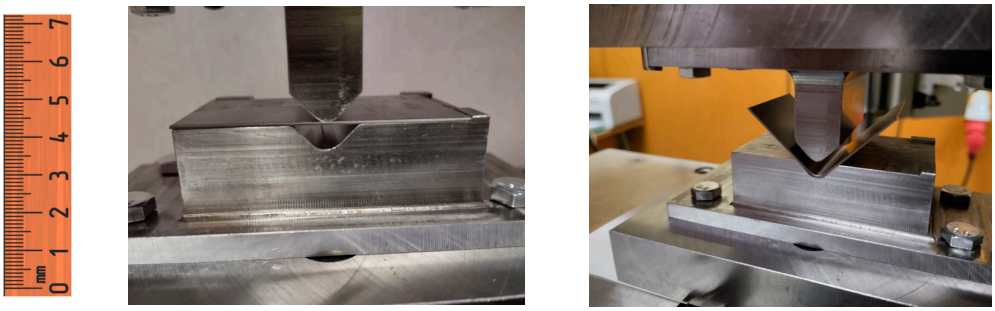

(**a**) (**b**)

Figure 8. Sheet specimen before and after air-bending.

The experiments were conducted on a Zwick/Roell Z100 universal testing machine under force-controlled conditions. The maximum forming force was prescribed in the TestXpert control software, and punch motion was stopped automatically once the target force was reached. A constant crosshead speed of 5 mm/min was used in all tests, ensuring

quasi-static conditions. Four force levels were investigated: 600 N, 1000 N, 1500 N, and 2000 N. This range was selected to cover low to moderate bending severities while remaining representative of forming conditions relevant for polymer-based tools in later stages of the study.

3.1.2. Optical Measurement of Bending Angles

After bending, all specimens were measured using optical 3D scanning based on structured light projection. A DAVID SLS-2 scanner was used to acquire dense point clouds of the bent sheets. Prior to scanning, the system was calibrated and the sheet surfaces were lightly matted to improve optical contrast (Figure 9). The bending angle was extracted from the scanned geometry using Geomagic Design X software (v2022) by generating a cross-section of the point cloud and fitting reference lines to the planar regions of the sheet legs.

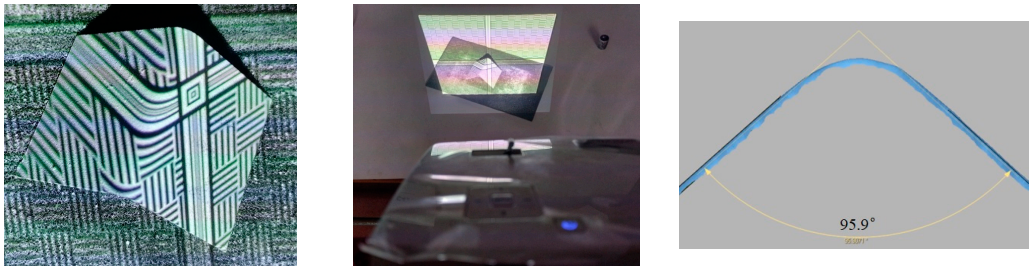

(**a**) (**b**) (**c**)

Figure 9. Optical 3D scanning of the bent specimen: (**a**) matted bent specimen; (**b**) David SLS-2 scanning; (**c**) cross section of point cloud and reference lines for sheet legs.

To exclude potential measurement bias due to fixture tolerances or alignment errors, the measured angles were additionally verified using a mechanical goniometer. The experimentally measured bending angles for all force levels are summarized in Table 3. Excellent agreement was observed between optical and mechanical measurements, confirming the reliability of the adopted measurement methodology.

Table 3. Experimentally measured bending angles.

Forming Load (N)	Bent Angle (Scanner)	Bent Angle (Goniometer)	Difference
600	95.89°	96°	0.11°
1000	93.64°	93.5°	0.14°
1500	93.18°	93.2°	0.02°
2000	92.51°	92.5°	0.01°

3.1.3. Comparison with Numerical Simulation Using Rigid Tools

To verify the accuracy of the numerical model and the experimentally determined material properties, the experimental results were compared with finite element simulations performed using rigid tools. The comparison focused on two key quantities: (i) the force–displacement response and (ii) the bending angle after elastic unloading (springback).

Figure 10 presents the numerical setup of the air-bending process together with the deformed sheet after unloading, illustrated by the distribution of effective plastic strain. The simulations were carried out using a two-dimensional planar model, which is appropriate for air bending due to the constant cross-section along the bending length. After completion of the forming stage, elastic unloading was simulated by removing both the punch and die. This unloading phase was defined in the *Sub-stages* module of Simufact.forming, where tool

release and workpiece relaxation were performed incrementally over ten steps to ensure numerical stability. The total strain variable, consisting of elastic and plastic components, was monitored throughout the process.

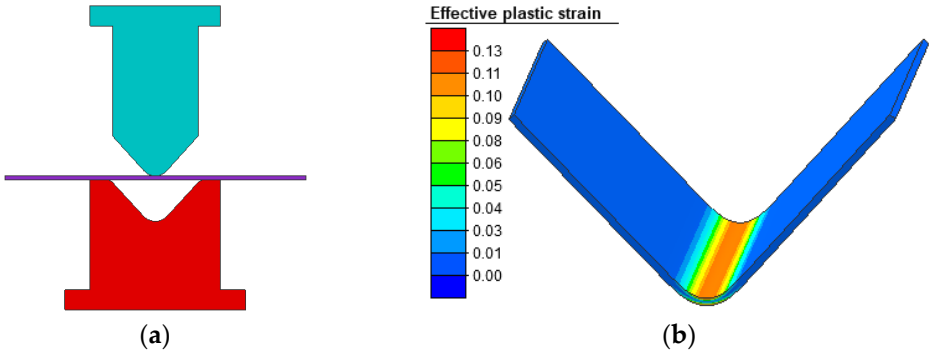

Figure 10. Numerical simulation of the air-bending process with rigid tools: (**a**) finite element model and boundary conditions; (**b**) deformed sheet after unloading with distribution of effective plastic strain.

The geometry of the bent sheet after elastic recovery was exported in STL format and evaluated in CAD software in order to determine the predicted bending angle. This procedure enabled a direct and consistent comparison with experimentally measured angles obtained from optical 3D scanning.

Figure 11 shows the experimental and numerical force–displacement curves for all four prescribed force levels (600 N, 1000 N, 1500 N, and 2000 N). Very good agreement between experimental and numerical curves was observed throughout the loading phase, indicating that the constitutive description of the sheet material and the defined contact conditions were appropriate.

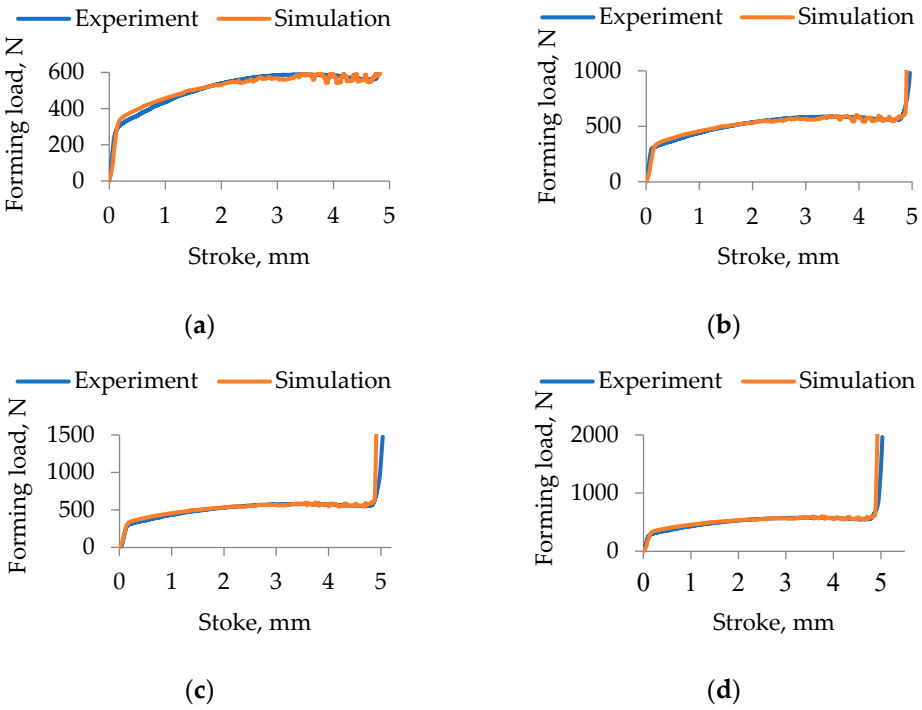

Figure 11. Experimental and numerical force–displacement curves with limited forming load: (**a**) 600 N; (**b**) 1000 N; (**c**) 1500 N; (**d**) 2000 N.

The predicted bending angles after springback were compared with experimentally measured values, as summarized in Table 4. The deviations between experimental and numerical results remained below 5% for all force levels, with the smallest discrepancy observed at the lowest force level of 600 N. This behaviour is consistent with the reduced influence of calibration effects and frictional variability at lower forming forces.

Table 4. Comparison of bending angles.

Forming Load (N)	Bending Angle (Experiment)	Bending Angle (Numerical Simulation)	Difference
600	95.89°	96.33°	0.46%
1000	93.64°	94.66°	1.08%
1500	93.18°	94.42°	1.31%
2000	92.51°	93.46°	1.02%

Overall, these results confirm that the numerical model with rigid tools provides an accurate representation of the air-bending process, both in terms of global force–displacement response and springback prediction. The validated rigid-tool model therefore serves as a reliable reference framework for subsequent numerical analyses involving deformable tools and for the determination of springback compensation angles.

3.2. Numerical Analysis with Deformable Tools

After validation of the numerical model using rigid tools, additional finite element analyses were performed with deformable punch and die in order to quantify the elastic response of the tools under forming loads. This step is particularly relevant when considering polymer-based tooling, where reduced tool stiffness may influence the force–displacement response and indirectly affect the resulting bending angle.

3.2.1. Two-Dimensional FEM with Deformable Tools

After validation of the numerical model using rigid tools, the air-bending process was further analysed using a two-dimensional planar finite element model with deformable punch and die. The same geometric configuration, boundary conditions, material models, and contact definitions as in the rigid-tool simulations were retained, enabling direct comparison between the two modelling approaches. The forming force was limited to the same four levels (600 N, 1000 N, 1500 N, and 2000 N), consistent with the experimental program and with the load range relevant for additively manufactured polymer tools.

The punch and die were discretized using an advancing-front quadrilateral finite element mesh with Quad 11 elements. A nominal element size of 2 mm was adopted for the tool bodies. In order to accurately capture stress gradients and elastic deformation in regions of intensive tool–sheet interaction, the mesh was locally refined in the contact zones using refinement boxes with a refinement factor of four. The resulting finite element meshes for the deformable punch and die are shown in Figure 12. The tool material was defined as steel C60, as in experimental tool, taken from the Simufact.forming material database, and modelled as linear elastic.

The bending process was simulated under force-controlled conditions. After reaching the prescribed maximum forming force, elastic unloading was simulated by removing both tools and allowing the sheet to relax incrementally over ten unloading steps. This unloading procedure was defined within the *Sub-stages* module of Simufact.forming, using the options *Release dies attached to press* and *Release workpiece from stationary dies*. The total strain variable, composed of elastic and plastic components, was monitored throughout the unloading phase.

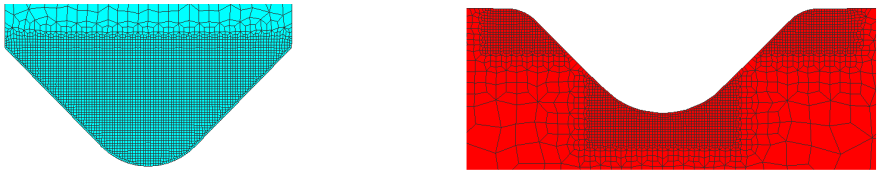

(**a**) (**b**)

Figure 12. Locally refined finite element mesh (refinement boxes) applied to: (**a**) the punch and (**b**) the die.

A representative force–displacement curve obtained from the simulation with deformable tools for the maximum forming force of 600 N is shown in Figure 13. The numerical response confirms stable process behaviour and is consistent with the corresponding experimental observations.

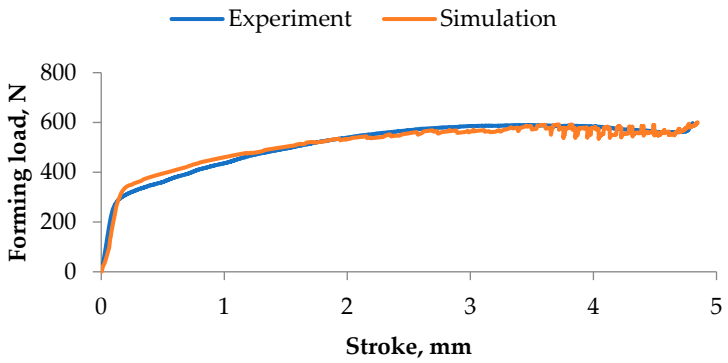

Figure 13. Force–displacement response obtained from the numerical simulation with deformable tools, maximum forming force 600 N (compared with experimental diagram).

The results of the numerical simulations with deformable tools are in full agreement with the experimental findings, indicating that no damage or permanent deformation occurs in the punch or die within the investigated force range. The predicted tool deformations are purely elastic and of very small magnitude, confirming that steel tools behave effectively as rigid bodies under the applied loading conditions. This finding provides a sound numerical basis for extending the analysis to polymer-based tools, where lower stiffness may lead to slightly increased elastic deformation without compromising structural integrity.

3.2.2. Stress State, Contact Pressure, and Elastic Tool Deformation

To assess the mechanical response of the deformable tools in more detail, the distributions of effective stress, contact pressure, and elastic deformation were analysed for the maximum forming force of 600 N. The results for the die are shown in Figure 14, while the corresponding results for the punch are presented in Figure 15.

For the die, the maximum effective stress reached approximately 70 MPa and was confined to a very small region near the contact radius. Similarly, the maximum contact pressure was localized in the regions where continuous contact between the sheet and the die occurred throughout bending. The predicted elastic deformation of the die was extremely small, on the order of one micrometre, indicating that the tool operates well within the elastic regime.

A comparable response was observed for the punch. The maximum effective stress and contact pressure were slightly higher than those in the die but remained localized and well below critical levels. The maximum elastic deformation of the punch was below 0.5 μm. These results confirm that, under the investigated loading conditions, the steel tools experience only minor elastic deflection and no permanent deformation.

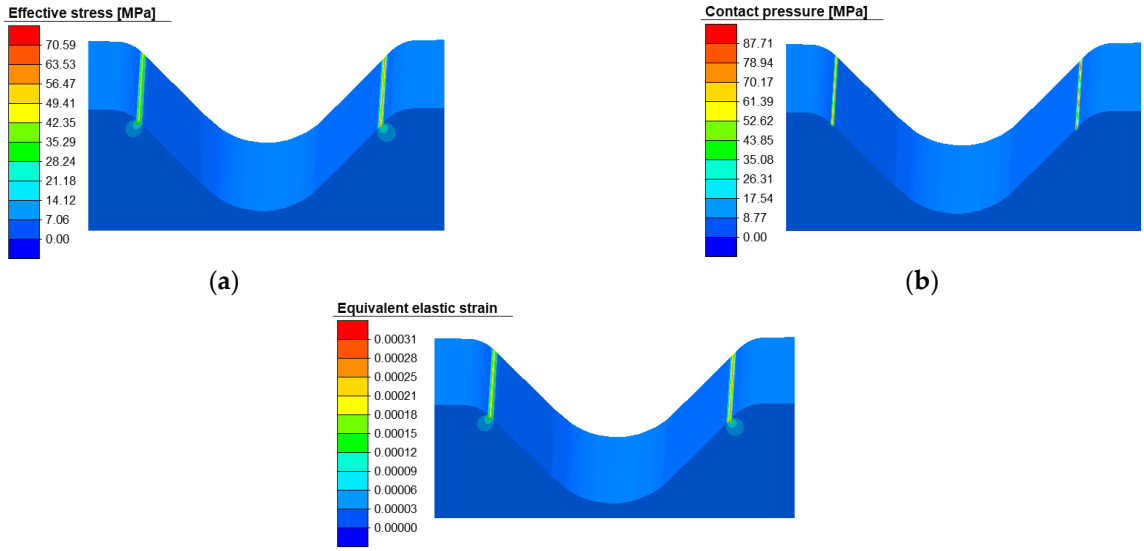

Figure 14. Distribution of results on the deformable die at a maximum forming force of 600 N: (**a**) equivalent (von Mises) stress; (**b**) contact pressure; (**c**) elastic deformation.

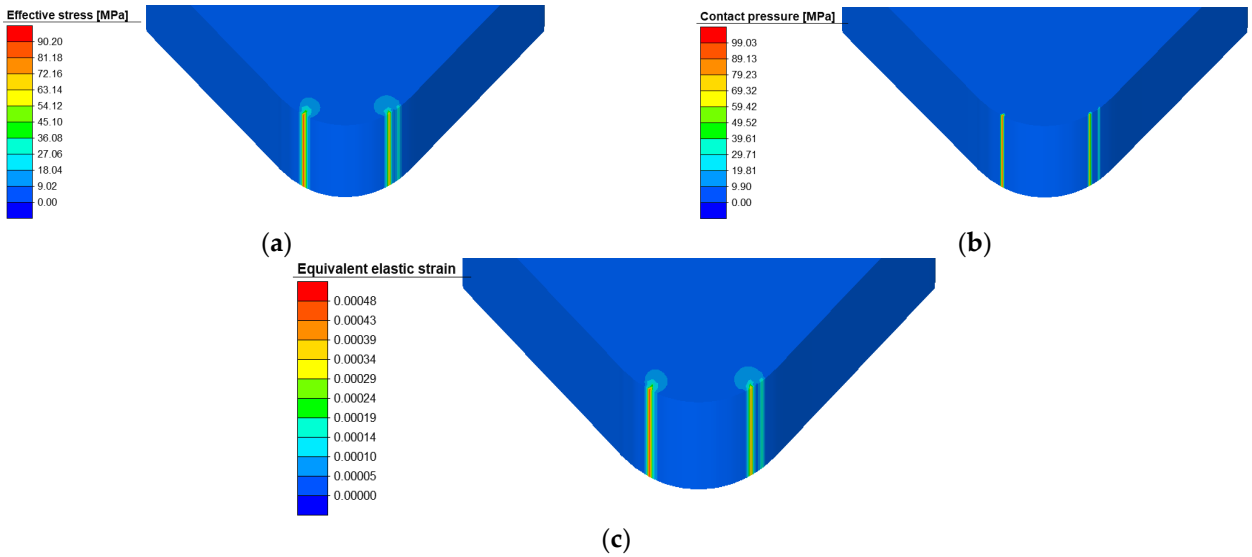

Figure 15. Distribution of results on the deformable punch at a maximum forming force of 600 N: (**a**) equivalent (von Mises) stress; (**b**) contact pressure; (**c**) elastic deformation.

The localized peaks observed in stress and contact pressure distributions can be attributed to numerical concentration effects associated with contact discretization and are not indicative of global tool overloading. Overall, the two-dimensional simulations with deformable tools demonstrate that elastic deformation of metallic tools has a negligible influence on the bending response within the applied force range.

3.2.3. Three-Dimensional FEM Verification

To further validate the numerical approach, a three-dimensional finite element simulation of the air-bending process was performed using deformable tools. The sheet was discretized using a *Sheetmesh* with hexahedral elements of nominal size 0.5 mm, with local mesh refinement in the bending zone using refinement boxes. The punch and die were discretized using tetrahedral elements (type 134), which are well suited for evaluating

elastic deformation in tooling components. Local mesh refinement was also applied in the contact regions of both tools.

As in the two-dimensional simulations, the forming force was limited to 600 N, and elastic unloading was simulated over ten incremental steps after tool removal. The resulting force–displacement curve obtained from the three-dimensional simulation is shown in Figure 16 and exhibits very good agreement with the corresponding two-dimensional results.

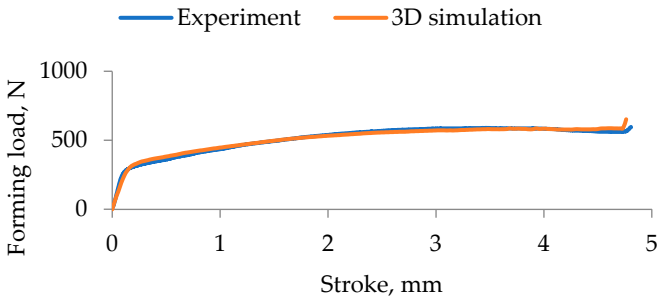

Figure 16. Force–displacement curve obtained from 3D numerical simulation (compared with experimental curve).

The predicted bending angle after elastic unloading obtained from the 2D simulation with deformable tools was 96.20°, corresponding to a deviation of only 0.32% with respect to the experimentally measured value. The 3D simulation with deformable tools yielded a bending angle of 96.28°, resulting in a deviation of 0.41%. These results indicate that the 2D finite element model with deformable tools provides the smallest deviation from experimental measurements among the investigated numerical approaches.

Importantly, the 2D deformable-tool model achieves this level of accuracy at a fraction of the computational cost required for the corresponding 3D simulations. This confirms that the proposed two-dimensional formulation represents a numerically efficient and sufficiently accurate approach for springback prediction and evaluation of tool stiffness effects in air-bending processes, making it particularly suitable for iterative design and optimization of additively manufactured polymer tools.

These results demonstrate that the numerical model reliably captures both sheet springback and elastic tool deformation and can therefore be confidently used in subsequent stages of the study, including springback compensation, redesign of tool angles, and analysis of additively manufactured polymer tools.

3.2.4. Implications for Tool Design and Model Reliability

Comparison of experimental results with numerical predictions obtained using rigid tools, two-dimensional deformable tools, and three-dimensional deformable tools demonstrated that the differences in predicted bending angles remain below approximately 1.5% across all investigated cases. The smallest deviations were observed at the lowest forming force level of 600 N, which is particularly relevant for polymer-based bending tools operating under low-force conditions.

These findings confirm that elastic deformation of steel tools has a negligible influence on springback within the investigated force range and that the validated numerical framework provides a reliable basis for springback prediction and angle compensation. In particular, the two-dimensional model with deformable tools achieves the highest accuracy with significantly reduced computational cost compared to the corresponding three-dimensional simulations.

Consequently, the proposed modelling approach can be confidently applied to the analysis and design of additively manufactured polymer tools, where reduced tool stiffness

compared to metallic tools may influence the effective bending response and where efficient numerical iteration is essential for accurate springback compensation.

3.3. Springback Compensation and Tool Angle Correction

3.3.1. Numerical Estimation of the Compensation Angle

The springback compensation angle was determined by means of finite element simulations following the numerical plan summarized in Table 5. Several punch–die angle configurations were investigated in order to identify the tool geometry that results in a final bending angle as close as possible to the target value of 90° after elastic unloading. Based on preliminary numerical analyses, the die angles were varied between 84°, 85°, and 86°. For each die angle, two configurations were analysed: (i) one in which the punch angle was 1° smaller than the die angle, and (ii) one in which the punch and die angles were equal. In total, six numerical experiments were performed.

Table 5. Numerical experiment plan for springback compensation.

Numerical Experiment	Punch and Die Angle Combinations	Die Angle α_m	Punch Angle α_o
1	1.1	84°	83°
	1.2	84°	84°
2	2.1	85°	84°
	2.2	85°	85°
3	3.1	86°	85°
	3.2	86°	86°

The punch radius was fixed at 3.2 mm, while the die radius was 4 mm. The geometric definitions of the punch and die are shown in Figure 17.

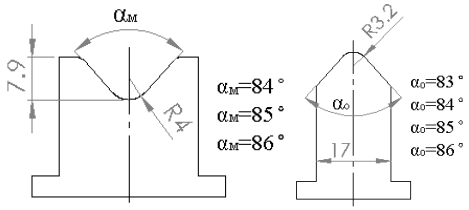

Figure 17. Geometry of the punch and die used for numerical springback compensation analysis.

The bending angle of the virtual sheet after elastic unloading was evaluated by exporting the deformed geometry from Simufact.forming in STL format and measuring the angle in Geomagic Design X. A cross-section of the virtual bent part was extracted using the *Mesh Sketch* function, and the bending angle was determined from the fitted reference lines, as illustrated in Figure 18. The numerically estimated bending angles after unloading for all investigated configurations are summarized in Table 6.

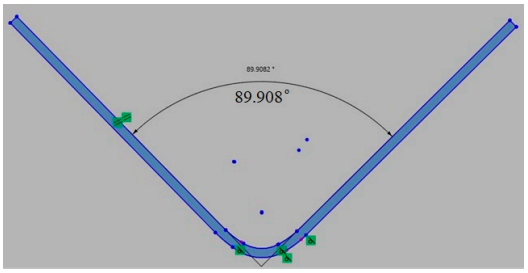

Figure 18. Measuring the bending angle on a virtual bent part in *Geomagic design* software (v2022).

Table 6. Numerically estimated bending angles after unloading.

Numerical Experiment	Punch and Die Angle Combinations	Numerically Estimated Bending Angles	Difference From 90°
1	1.1	88.94°	1.06°
	1.2	88.89°	1.11°
2	**2.1**	**89.89°**	**0.11°**
	2.2	**89.90°**	**0.10°**
3	3.1	90.91°	0.91°
	3.2	90.78°	0.78°

The results indicate that the highest accuracy was obtained for two configurations: (2.1) a die angle of 85° combined with a punch angle of 84°, and (2.2) equal punch and die angles of 85°. In both cases, the predicted bending angle after springback was very close to the target value of 90°.

3.3.2. Experimental Verification of the Compensated Tool Geometry

Experimental verification of the numerically determined compensation angle was performed using a modified steel tool with compensated punch and die angles of 85°. The experiments were carried out with five repetitions under identical process conditions. Bending angles were measured using optical 3D scanning with the DAVID SLS-2 structured-light scanner, following the same procedure described in Section 2.5.2. The measured angles were compared with numerically predicted values, and the results are summarized in Table 7.

Table 7. Experimental verification of springback compensation.

Experiment	Measured Bending Angles	Numerically Estimated Bending Angles	Difference
1	89.83°	88.90°	−0.07°
2	89.40°	88.90°	−0.50°
3	89.31°	89.90°	−0.59°
4	89.39°	89.90°	−0.51°
5	89.73°	89.90°	−0.17°
Average	**89.53°**	**89.90°**	**−0.37°**

The average measured bending angle was 89.53°, corresponding to a mean deviation of −0.40% relative to the numerically predicted value. These deviations are well within acceptable limits for sheet metal bending. According to established guidelines, expected angular deviations in air bending are on the order of ±1°. Possible sources of the remaining discrepancies include material variability of DC04 steel (non-guaranteed chemical composition) and accumulated measurement uncertainties associated with optical scanning and surface preparation.

3.3.3. Discussion and Implications for Tool Design

The combined numerical and experimental results demonstrate that the proposed finite element-based compensation strategy enables highly accurate prediction and correction of springback in air bending. The average angular deviation of approximately 0.4% confirms the reliability of the numerical model and its suitability for tool angle correction.

Since the validated numerical framework accurately captures the elastic springback behavior of the sheet under low-force bending conditions, it can be directly applied to the design of additively manufactured polymer tools. The model provides a robust basis for numerical determination of tool angle compensation required to counteract sheet

springback and to account for the reduced stiffness of polymer tools, which is addressed in the subsequent section.

3.4. Air Bending with Additively Manufactured ABS Tools

3.4.1. Additive Manufacturing of ABS Tool Components

Based on the numerical springback compensation strategy established in Sections 3.2 and 3.3, the final geometry of the bending tools was defined with a compensated die angle of 85° and a punch angle of 84°. This configuration was selected to avoid unintended double-sided contact between the sheet and the tool flanks while maintaining numerical accuracy, as the deviation from the optimal numerical solution was below 0.02°.

The punch and die inserts were manufactured from ABS using material extrusion AM (MEX). STL files were generated from the CAD models in CATIA using the *Machining—STL Rapid Prototyping* module. The tessellation parameters were carefully selected to minimize geometric deviation between the CAD model and the STL representation. A sag value of 0.01 mm was adopted, representing the maximum allowable distance between the nominal geometry and the triangulated surface, while the step parameter was set to 0.2 mm to control triangle edge length.

The ABS tool components were printed on a MakerBot Replicator 2X printer. To minimize dimensional deviations related to anisotropic printing accuracy in the X–Y plane, the punch and die were printed simultaneously in the same build job and orientation. The printing parameters were selected based on the material characterization presented in Section 2.2 and are summarized as follows: layer thickness 0.1 mm, raster orientation ±45°, printing speed 55 mm/s, and 100% infill density. After printing, the parts were removed from the build platform, the raft was removed, and functional mounting surfaces were lightly polished to ensure proper assembly and alignment. The final appearance of the additively manufactured ABS punch and die after post-processing, mounted in the bending tool is shown in Figure 19.

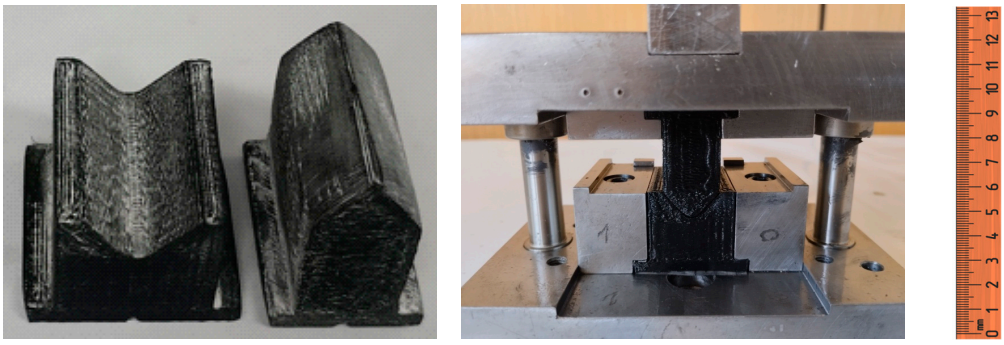

(**a**) (**b**)

Figure 19. Additively manufactured ABS tool: (**a**) punch and die after post-processing; (**b**) mounted ABS components in the bending tool.

3.4.2. Numerical Assessment of ABS Tools Prior to Manufacturing

Before experimental testing, finite element simulations of the air-bending process with ABS tools were performed to verify tool integrity, stress levels, and dimensional accuracy of the bent sheet. The simulations aimed to confirm that the additively manufactured tools could withstand the applied loads without damage and that the compensated geometry would result in the desired bending angle.

The ABS material behavior was modeled using the experimentally determined flow curve obtained from tensile tests on fully filled specimens. The flow stress was described

using a power-law relationship with parameters C = 1314.59 MPa and n = 1.073. The ABS tools were modelled as deformable bodies, while the sheet material and contact conditions were defined consistently with the validated numerical framework used in previous sections.

The simulations demonstrated that bending with ABS tools is feasible within the investigated force range (600 N). The distribution of elastic and plastic deformation on the ABS punch obtained from numerical simulation is presented in Figure 20. The results indicate that deformation remains localized near the punch radius and is predominantly elastic. The corresponding distributions of contact pressure and effective stress on the ABS punch are shown in Figure 21.

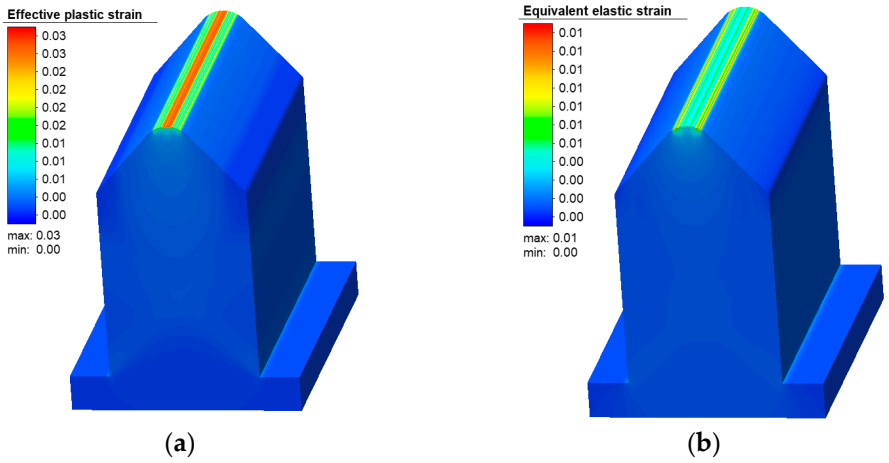

Figure 20. Distribution of strains on the ABS punch: (**a**) effective plastic; (**b**) equivalent elastic.

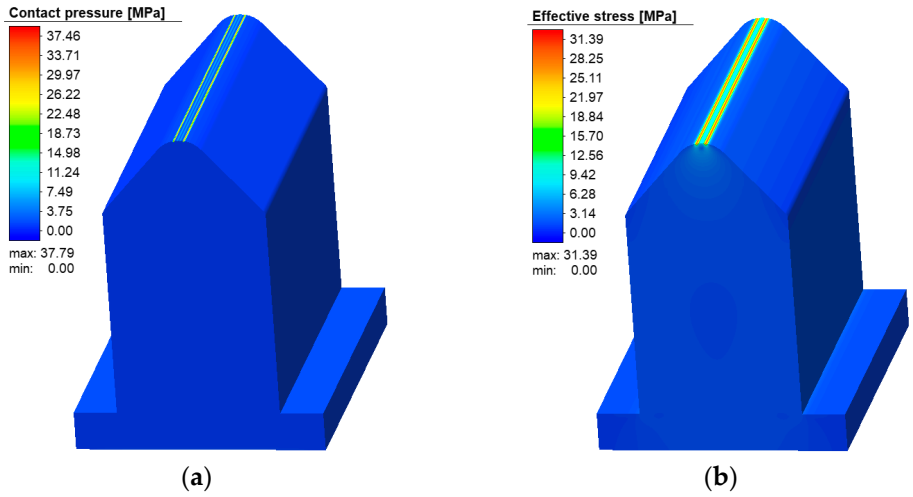

Figure 21. Distribution of contact pressure (**a**) and effective stress (**b**) on the ABS punch.

Stress and deformation fields showed that tool deformation remained localized and elastic. The maximum contact pressure on the punch reached approximately 37 MPa, while the peak effective stress was below 32 MPa. The highest deformation levels were observed near the punch radius and were confined to a very small region, indicating no risk of tool failure.

Similarly, the die exhibited low stress and deformation levels. Stress and deformation results for the ABS die are shown in Figures 22 and 23. The maximum contact pressure on the die was approximately 50 MPa, and the maximum effective stress remained below 40 MPa. Localized plastic strain was observed only in a very small area near the die radius and was attributed to numerical approximation effects rather than actual material yielding.

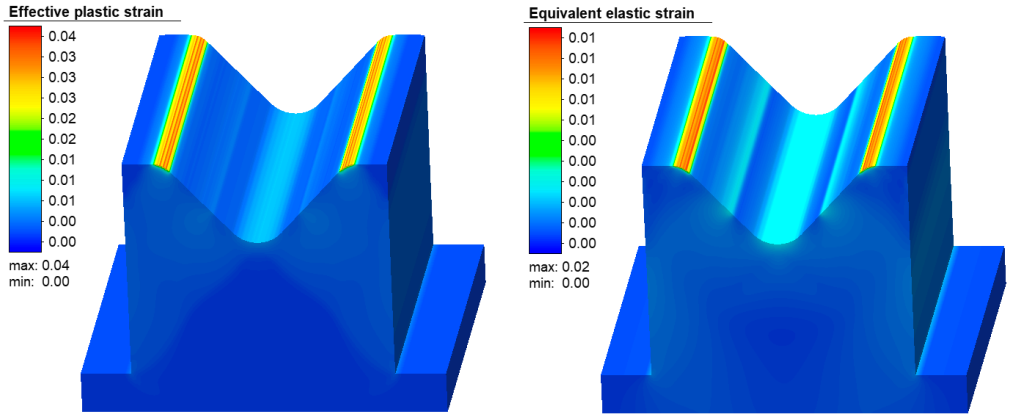

Figure 22. Distribution of strains on the ABS die: (**a**) effective plastic; (**b**) equivalent elastic.

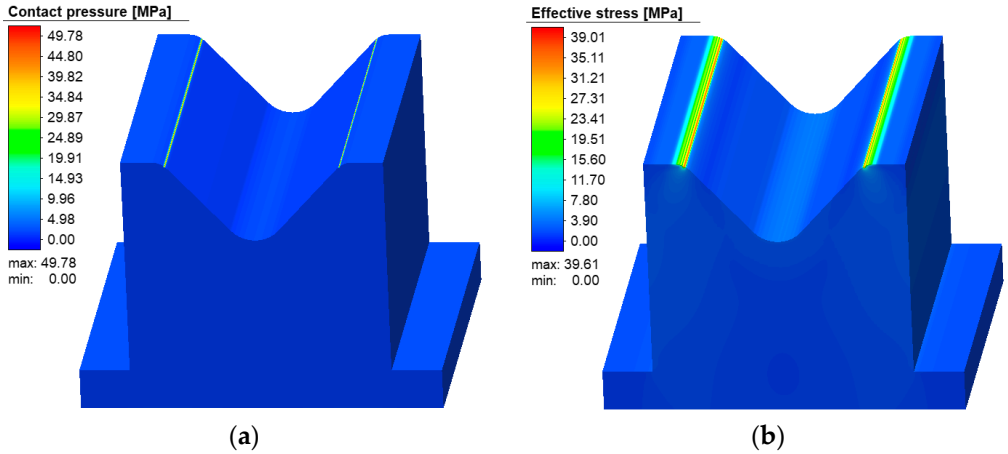

Figure 23. Distribution of contact pressure (**a**) and effective stress (**b**) on the ABS die.

Overall, the numerical analysis confirmed that the additively manufactured ABS tools possess sufficient stiffness and load-bearing capacity for the intended air-bending operation with compensated tool geometry.

3.4.3. Experimental Air-Bending Tests with ABS Tools

Experimental air-bending tests were subsequently conducted using the additively manufactured ABS punch and die mounted in the same modular tool system previously used for metallic tools. The experiments were performed on a Zwick/Roell Z100 universal testing machine under force-controlled conditions, with the maximum forming force limited to 600 N. A view of the ABS tool mounted on the testing machine at the beginning and during the bending process is shown in Figure 24.

Five repeated bending experiments were carried out under identical conditions. During each test, force–displacement data were recorded using the TestXpert software. A direct comparison between force–displacement responses obtained with metallic tools and ABS tools is shown in Figure 25. While the overall trends are similar, slight differences in force levels were observed in some ABS tool experiments due to increased friction effects, which led to earlier attainment of the prescribed maximum force and slightly reduced punch stroke. This effect resulted in marginally larger bending angles after unloading.

The bent specimens were measured using optical 3D scanning based on structured light, following the same procedure described in Section 2.5. The measured bending angles were compared with numerical predictions obtained from simulations using compensated tool geometries.

(**a**) (**b**)

Figure 24. ABS tool mounted on the machine: (**a**) at the beginning and (**b**) during the air-bending process.

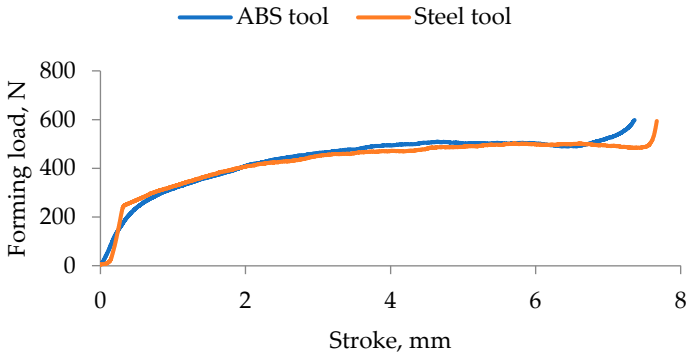

Figure 25. Comparison of force–displacement responses for metallic and ABS bending tools.

3.4.4. Validation of Springback Compensation with ABS Tools

The experimentally measured bending angles obtained with ABS tools showed very good agreement with numerically predicted values. The results of this comparison are summarized in Table 8.

Table 8. Measured bending angles obtained with ABS tools and comparison with metallic tools and numerical predictions.

Exp.	Bending Angles (ABS Tools)	Bending Angles (Metallic Tools)	Difference (ABS vs. Metallic)	Numerically Estimated Angles	Difference (ABS vs. Numerical)
1	90.27°	89.83°	0.44°	88.90°	0.37°
2	90.20°	89.40°	0.80°	88.90°	0.30°
3	90.52°	89.31°	1.21°	89.90°	0.62°
4	90.43°	89.39°	1.04°	89.90°	0.53°
5	90.77°	89.73°	1.04°	89.90°	0.87°
Aver.	**90.43°**	**89.53°**	**0.90°**	**89.90°**	**0.59°**

Across the five repeated experiments, the average measured bending angle was 90.43°, compared to the numerically predicted value of 89.89°, resulting in an average deviation of 0.61%. This level of accuracy is well within acceptable limits for air-bending operations and is consistent with reported industrial tolerances of ±1°.

No visible damage, cracking, or permanent deformation of the ABS tools was observed during or after testing. The results confirm that additively manufactured ABS tools, when designed using a validated numerical springback compensation strategy, can successfully replace metallic tools for low-force air-bending operations.

Minor discrepancies between experimental and numerical results were attributed to the inherent dimensional tolerance of MEX printing, friction effects in the guiding system, small

variations in sheet thickness, and assembly related uncertainties. Nevertheless, the overall agreement confirms the robustness of the proposed numerical–experimental framework.

4. Discussion

The present study aimed to develop and validate an integrated experimental–numerical framework for air bending of sheet metal using additively manufactured polymer tools, with particular emphasis on springback prediction and tool angle compensation. The discussion below interprets the obtained results in the context of previous studies and highlights their broader implications for additive tooling in bending operations.

4.1. Validation of the Experimental–Numerical Framework

The comparison between experimental results obtained with conventional steel tools and finite element simulations using rigid tools demonstrated very good agreement in terms of force–displacement response and bending angle after elastic unloading. The deviations between experimentally measured and numerically predicted bending angles ranged from 0.46% to 1.31% for all investigated forming loads, with the smallest deviation observed at the lowest force level of 600 N. These results confirm that the adopted constitutive models, contact definitions, and unloading strategy provide an accurate representation of the air-bending process. The observed level of agreement is consistent with previous numerical studies on springback prediction in air bending, which emphasize the importance of reliable material characterization and controlled elastic unloading procedures.

The extension of the numerical analysis to deformable steel tools further confirmed that elastic deformation of the tools has a negligible influence on the final bending angle within the investigated force range. The predicted bending angle after elastic unloading obtained from the two-dimensional simulation with deformable tools was 96.20°, corresponding to a deviation of only 0.32% with respect to the experimentally measured value. The three-dimensional simulation with deformable tools yielded a bending angle of 96.28°, resulting in a deviation of 0.41%. These results demonstrate that the 2D finite element model with deformable tools provides the smallest deviation from experimental measurements among the investigated numerical approaches, while requiring significantly lower computational effort than full 3D simulations. This confirms that air bending of thin sheets can be reliably treated as a planar process for the purpose of springback prediction and tool angle compensation.

4.2. Implications for Springback Compensation

The numerical investigation of springback compensation demonstrated that systematic variation in punch and die angles enables accurate control of the final bending angle without relying on empirical trial-and-error adjustments. The identified optimal tool configurations resulted in predicted bending angles very close to the target value of 90°, with deviations well within typical industrial tolerances. Experimental verification using compensated steel tools confirmed the reliability of the numerical predictions, with average angle deviations of approximately 0.4%, which is substantially lower than the commonly accepted $\pm 1^\circ$ tolerance in sheet metal bending.

These results highlight the importance of combining validated numerical models with controlled experiments for springback compensation. Unlike many previous studies where compensation strategies are applied empirically, the present approach provides a rational and transferable methodology that can be applied to different materials, tool geometries, and forming conditions.

4.3. Performance of Additively Manufactured ABS Tools

Numerical simulations performed prior to manufacturing the polymer tools demonstrated that ABS tools with compensated angles can safely withstand the applied forming loads, with stress and deformation levels remaining below critical values. The experimental air-bending tests using additively manufactured ABS tools confirmed these predictions: no visible damage or excessive deformation of the tools was observed, and the resulting bending angles showed good repeatability across multiple experiments.

The comparison between metal and ABS tools revealed slightly larger deviations in force–displacement curves and bending angles for the polymer tools, which can be attributed primarily to their lower structural stiffness compared to steel tools, manufacturing tolerances inherent to the MEX AM process, and friction effects in the guiding system. Nevertheless, the average deviation between experimentally measured and numerically predicted bending angles for ABS tools remained below 1%, demonstrating that the validated numerical framework is capable of accurately predicting sheet springback and the resulting final bend angle even when additively manufactured polymer tools are used.

In comparison with previous feasibility-focused studies on polymer bending tools, the present work goes beyond demonstrating that polymer tools "work" and instead provides a predictive framework for tool design and compensation. This represents an important step toward more systematic and reliable use of additive tooling in bending operations.

4.4. Limitations and Directions for Future Research

Although the proposed methodology has been successfully validated for ABS tools under low forming forces, several aspects warrant further investigation. First, the current study focused on fully solid polymer tools to ensure sufficient stiffness and strength. Future work should explore the application of topology optimization to reduce material consumption and printing time while maintaining acceptable tool stiffness and dimensional accuracy. The numerical stress and deformation data obtained in this study provide a solid basis for such optimization.

Second, the present validation was performed under controlled laboratory conditions using a limited range of forces and sheet thickness. Extending the methodology to more complex bending sequences, higher force levels, and different sheet materials would further clarify the applicability limits of polymer tools. In particular, validation on industrial press brakes and multi-operation bending processes would provide valuable insight into the robustness of the proposed approach under realistic production conditions.

Finally, further refinement of constitutive models for additively manufactured polymers, including anisotropy, rate dependence, and damage evolution, would improve the predictive capability of numerical simulations, especially for long-term tool durability and repeated loading scenarios.

5. Conclusions

This paper presented a comprehensive experimental–numerical framework for the analysis of air bending of sheet metal using additively manufactured polymer tools. The proposed methodology integrates detailed material characterization, finite element modelling with rigid and deformable tools, controlled bending experiments, and high-resolution optical measurements to achieve accurate prediction and compensation of springback. By systematically validating the numerical models against experimental results obtained with both metallic and polymer tools, the study establishes a reliable basis for rational tool design and springback control in low-force air-bending applications.

The main conclusions of the study can be summarized as follows:

- Accurate characterization of the mechanical behaviour of both the sheet material (DC04 steel) and the polymer tool material (MEX-printed ABS) is essential for reliable numerical prediction of air-bending behaviour and springback.
- Finite element simulations using rigid steel tools showed very good agreement with experimental results, with deviations in bending angle ranging from 0.46% to 1.31%, confirming the validity of the adopted material models, contact conditions, and unloading strategy.
- Numerical analyses with deformable steel tools demonstrated that elastic tool deformation has a negligible influence on springback within the investigated force range. The two-dimensional deformable model provided the smallest deviation from experimental measurements (0.32%) while requiring significantly lower computational effort than three-dimensional simulations.
- The validated numerical framework enabled reliable determination of springback compensation angles. Experimental verification of the compensated tool geometry showed an average angular deviation of approximately 0.4%, well within acceptable tolerances for air-bending operations.
- Air-bending experiments performed with additively manufactured ABS tools confirmed that polymer tools can successfully replace conventional steel tools under low-force conditions. The average deviation between experimentally measured and numerically predicted bending angles was approximately 0.6%, demonstrating the practical applicability of the proposed methodology.

Overall, the results confirm that a properly validated experimental–numerical approach allows accurate prediction and compensation of springback in air bending with additively manufactured polymer tools. The presented framework provides a robust methodological basis for the design and assessment of polymer bending tools and can significantly reduce tooling cost and lead time in low-volume and flexible manufacturing scenarios.

Future research will focus on extending the proposed approach to topologically optimized polymer tools, investigating durability and wear over extended forming cycles, and validating the methodology on industrial press brake applications involving multi-step bending operations and more complex part geometries.

Author Contributions: Conceptualization, V.M. and M.D.; methodology, V.M.; validation, V.M., M.D. and D.A. (Dragan Adamovic); formal analysis, D.A. (Dusan Arsic); investigation, M.D.; resources, V.M.; data curation, V.M., M.D. and A.I.; writing—original draft preparation, V.M.; writing—review and editing, N.R.; visualization, D.I.; supervision, D.A. (Dragan Adamovic); project administration, D.A. (Dusan Arsic) and A.I.; funding acquisition, V.M. All authors have read and agreed to the published version of the manuscript.

Funding: This research was funded by the Ministry of Science, Technological Development and Innovation of the Republic of Serbia, grant number TR34002.

Data Availability Statement: The original data presented in the study are openly available in ZENODO repository at https://doi.org/10.5281/zenodo.18024091.

Conflicts of Interest: The authors declare no conflicts of interest.

Abbreviations

The following abbreviations are used in this manuscript:

ABS	Acrylonitrile–Butadiene–Styrene
AM	Additive Manufacturing
CAD	Computer Aided Design

DC04	Linear dichroism
FE	Finite Element
FDM	Fused Deposition Modelling
FFF	Fused Filament Fabrication
ISO	International Organization for Standardization
MEX	Material Extrusion
PLA	Polylactic Acid
R_p	Yield stress
R_m	Ultimate tensile strength
ε_f	Fracture strain
STL	Standard Tessellation Language

References

1. *ISO/ASTM 52900:2021*; Additive Manufacturing—General Principles—Fundamentals and Vocabulary. ISO/ASTM International: Geneva, Switzerland, 2021.
2. Nakamura, N.; Mori, K.; Abe, Y. Applicability of Plastic Tools Additively Manufactured by Fused Deposition Modelling for Sheet Metal Forming. *Int. J. Adv. Manuf. Technol.* **2020**, *108*, 975–985. [CrossRef]
3. Durgun, I. Sheet Metal Forming Using FDM Rapid Prototype Tool. *Rapid Prototyp. J.* **2015**, *21*, 412–422. [CrossRef]
4. Popovic, M.; Mandic, V.; Delic, M. Application of Techniques and Systems for Additive Manufacturing in Rapid Tooling. In Proceedings of the International Conference on Machine and Industrial Design in Mechanical Engineering, Novi Sad, Serbia, 10–12 June 2022; Springer: Cham, Switzerland, 2022; Volume 109, pp. 557–565. [CrossRef]
5. Kaleem, M.A.; Frohn-sörensen, P.; Steinheimer, R.; Engel, B. Design criteria to use 3D printed polymeric tools in metal forming processes. In Proceedings of the 44th Conference of the International Deep Drawing Research Group, MATEC Web Conference, Lisbon, Portugal, 1–5 June 2025; EDP Sciences: Les Ulis, France, 2025; Volume 408. [CrossRef]
6. Prithvirajan, R.; Sugavaneswaran, M.; Sathishkumar, N.; Arumaikkannu, G. Metal bellow hydroforming using additive manufactured die: A case study. *Rapid Prototyp. J.* **2021**, *25*, 765–774. [CrossRef]
7. Tondini, F.; Basso, A.; Arinbjarnar, U.; Nielsen, C.V. The Performance of 3D Printed Polymer Tools in Sheet Metal Forming. *Metals* **2021**, *11*, 1256. [CrossRef]
8. Tondini, F.; Arinbjarnar, U.; Basso, A.; Nielsen, C.V. 3D printing to facilitate flexible sheet metal forming production. *Procedia CIRP* **2021**, *103*, 91–96. [CrossRef]
9. Rehman, A.U. Additive Manufacturing of Plastic Tools for Sheet Metal Forming. *Tech. J.* **2022**, *27*, 37–44.
10. Giorleo, L.; Deniz, K.I. Polymer Tools Produced by Fused Filament Fabrication for Steel-Bending Process: Effect of Layering Orientation. *J. Manuf. Mater. Process.* **2024**, *8*, 243. [CrossRef]
11. Zaragoza, V.G.; Rane, K.; Strano, M.; Monno, M. Manufacturing and performance of 3D printed plastic tools for air bending applications. *J. Manuf. Proc.* **2021**, *66*, 460–469. [CrossRef]
12. Frohn-Sörensen, P.; Geueke, M.; Engel, B.; Löffler, B.; Bickendorf, P.; Asimi, A.; Bergweiler, G.; Schuh, G. Design for 3D Printed Tools: Mechanical Material Properties for Direct Polymer Additive Tooling. *Polymers* **2022**, *14*, 1694. [CrossRef] [PubMed]
13. Hmeidat, N.S.; Brown, B.; Jia, X.; Vermaak, N.; Compton, B. Effects of infill patterns on the strength and stiffness of 3D printed topologically optimized geometries. *Rapid Prototyp. J.* **2021**, *27*, 1467–1479. [CrossRef]
14. El-Deeb, I.S.; Esmael, E.; Ebied, S.; Diab, M.R.; Dekis, M.; Petrov, M.A.; Zayed, A.A.; Egiza, M. Optimization of Nozzle Diameter and Printing Speed for Enhanced Tensile Performance of FFF 3D-Printed ABS and PLA. *J. Manuf. Mater. Process.* **2025**, *9*, 221. [CrossRef]
15. Bhuiyan, M.Z.H.; Khanafer, K. Exploring the Nonlinear Mechanical Characteristics of 3D-Printed ABS with Varying Infill Densities. *J. Manuf. Mater. Process.* **2025**, *9*, 103. [CrossRef]
16. Delić, M.; Mandić, V.; Aleksandrović, S.; Arsić, D.; Ivković, D. Determination of the influence of FDM printing parameters on tensile strength and fracture occurrence of additively manufactured ABS material. *Int. J. Struct. Integr.* **2025**, *16*, 570–590. [CrossRef]
17. Mandić, V. *Physical and Numerical Modelling of Metal Forming Processes*, 1st ed.; Faculty of Engineering University of Kragujevac: Kragujevac, Serbia, 2012; pp. 1–363. ISBN 978-86-86663-88-7. (In Serbian)
18. Aksenov, L.B.; Kononov, I.Y. 3D Printed Plastic Tool for Al Thin-Sheet Forming. *IOP Conf. Ser. Earth Environ. Sci.* **2019**, *337*, 012053. [CrossRef]
19. Kella, C.K.; Mallick, P.K. Springback Behavior of Aluminum/Polypropylene/Aluminum Sandwich Laminates. *J. Manuf. Mater. Process.* **2022**, *6*, 152. [CrossRef]

20. Giorleo, L.; Deniz, K.I. Topology Optimization of Polymer-Based Bending Tools Manufactured via Additive Technology: Numerical and Experimental Validation. *J. Manuf. Mater. Process.* **2025**, *9*, 310. [CrossRef]
21. Bhatia, C.V.; Patel, D.R. Simulation and Experimental Study of the V-Bending Process for SS304 and AA6061 Sheets Using Additively Manufactured Tools. *Rapid Prototyp. J.* 2025; *in press*. [CrossRef]
22. *ISO 6892-1:2019*; Metallic Materials—Tensile Testing—Part 1: Method of Test at Room Temperature. International Organization for Standardization: Geneva, Switzerland, 2019.
23. Minitab Statistical Software. Available online: https://www.minitab.com/en-us/products/minitab/ (accessed on 16 December 2025).
24. Simufact Forming. Available online: https://hexagon.com/products/simufact-forming (accessed on 16 December 2025).
25. Maté-González, M.A.; Aramendi, J.; González-Aguilera, D.; Yravedra, J. Statistical Comparison between Low-Cost Methods for 3D Characterization of Cut-Marks on Bones. *J. Remote Sens.* **2017**, *9*, 873. [CrossRef]